Remote Sensing of Environment 113 (2009) 2089–2102

Contents lists available at ScienceDirect

Remote Sensing of Environment

journal homepage: www.elsevier.com/locate/rse

Estimating impervious surfaces from medium spatial resolution imagery using the self-organizing map and multi-layer perceptron neural networks

Xuefei Hu, Qihao Weng *

Center for Urban and Environmental Change, Department of Geography, Geology, and Anthropology, Indiana State University, USA
Center for Urban and Environmental Change, Department of Geography, Geology, and Anthropology, Indiana State University, Terre Haute, IN 47809, USA

ARTICLE INFO

Article history:
Received 18 December 2008
Received in revised form 10 April 2009
Accepted 10 May 2009

Keywords:
Impervious surface estimation
Self-organizing map
Multi-layer perceptron
ASTER
Multi-temporal imagery

ABSTRACT

The studies of impervious surfaces are important because they are related to many environmental problems, such as water quality, stream health, and the urban heat island effect. Previous studies have discussed that the self-organizing map (SOM) can provide a promising alternative to the multi-layer perceptron (MLP) neural networks for image classification at both per-pixel and sub-pixel level. However, the performances of SOM and MLP have not been compared in the estimation and mapping of urban impervious surfaces. In mid-latitude areas, plant phenology has a significant influence on remote sensing of the environment. When the neural networks approaches are applied, how satellite images acquired in different seasons impact impervious surface estimation of various urban surfaces (such as commercial, residential, and suburban/rural areas) remains to be answered. In this paper, an SOM and an MLP neural network were applied to three ASTER images acquired on April 5, 2004, June 16, 2001, and October 3, 2000, respectively, which covered Marion County, Indiana, United States. Six impervious surface maps were yielded, and an accuracy assessment was performed. The root mean square error (RMSE), the mean average error (MAE), and the coefficient of determination (R^2) were calculated to indicate the accuracy of impervious surface maps. The results indicated that the SOM can generate a slightly better estimation of impervious surfaces than the MLP. Moreover, the results from three test areas showed that, in the residential areas, more accurate results were yielded by the SOM, which indicates that the SOM was more effective in coping with the mixed pixels than the MLP, because the residential area prevailed with mixed pixels. Results obtained from the commercial area possessed very high RMSE values due to the prevalence of shade, which indicates that both algorithms cannot handle the shade problem well. The lowest RMSE value was obtained from the rural area due to containing of less mixed pixels and shade. This research supports previous observations that the SOM can provide a promising alternative to the MLP neural network. This study also found that the impact of different map sizes on the impervious surface estimation is significant.

1. Introduction

Land use/land cover (LULC) changes affect the cycling of water, carbon, and energy, and have been recognized as one of the most important factors for global environmental change. Urbanization is the major force that is driving LULC changes (Hasse & Lathrop, 2003), and the environmental impacts of urbanization are contributed mostly by impervious surfaces (Lee & Lathrop, 2006). An impervious surface refers to an anthropogenic surface that prevents water from infiltrating into soils (Arnold & Gibbons, 1996). The common types of impervious surfaces can be categorized into two primary components: the rooftops and the transport system (roads, sidewalks, and parking lots) (Schueler, 1994). The environmental impacts of impervious surfaces have been discussed in many previous studies (Galli, 1991; Schueler, 1994; Arnold & Gibbons, 1996; Slonecker et al., 2001; Lu & Weng, 2006; Yuan & Bauer, 2007), which include impacts on water cycling, water quality, erosion of construction sites, non-point source pollution, stream health, and the urban heat island effect. The impervious surface related environmental issues, as well as the increased concern about rapid urbanization worldwide, have aroused a surge of research interests in impervious surface studies.

Satellite remote sensing images have been massively applied for impervious surface estimation due to their relatively low cost and suitability for large area mapping (Bauer et al., 2004). Many methods had been applied successfully for impervious surface extraction in previous research, including spectral mixture analysis, regression tree, artificial neural network, multiple regression and sub-pixel classification (Civico & Hurd, 1997; Small, 2001; Flanagan & Civco, 2001; Wu & Murray, 2003; Small, 2003; Yang et al., 2003b,a; Wu, 2004; Bauer et al., 2004; Lu & Weng, 2006). Wu and Murray in 2003 developed a Linear Spectral Mixture Analysis model with four end members: high-albedo, low-albedo, vegetation, and soil. The model was successfully applied to

* Corresponding author. Tel.: +1 812 237 2255; fax: +1 812 237 8029.
E-mail address: qweng@indstate.edu (Q. Weng).

0034-4257/$ – see front matter © 2009 Elsevier Inc. All rights reserved.
doi:10.1016/j.rse.2009.05.014

ETM+ images. Yang et al. (2003b) used a regression tree model to map sub-pixel percent impervious surfaces. Civico and Hurd (1997) built a neural network based impervious surface model. Bauer et al. (2004) used regression to model the relationship between percent impervious surface and "tasseled cap" greenness, and then the model was used to estimate the percentage of impervious surfaces. Among all the techniques, Artificial neural networks (ANN) have been widely used due to its advantages over statistical methods, such as no assumption about the probabilistic models of data, robust in noisy environments, and the ability to learn complex patterns (Ji, 2000). Although many neural network models have been developed, the multi-layer perceptron (MLP) feed-forward neural network is widely used (Kavzoglu & Mather, 2003). MLP has been used in many different applications, which include: (1) land use/land cover classifications (Foody et al., 1997; Zhang & Foody, 2001; Kavzoglu & Mather, 2003); (2) change detection (Li & Yeh, 2002); and (3) water properties estimation (Schiller & Doerffer, 1999; Zhang et al., 2002; Corsini et al., 2003). Other applications include forest structure mapping (Ingram et al., 2005), under-storey bamboo mapping (Linderman et al., 2004), cloud detection (Jae-Dong et al., 2006), and mean monthly ozone prediction (Chattopadhyay & Bandyopadhyay, 2007). The neural networks approaches applied to impervious surface estimation are relatively new. MLP has been applied for impervious surface estimation (Chormanski et al., 2008; Mohapatra & Wu, 2007). Chormanski et al. (2008) conducted a multi-layer perceptron model to map the fractions of four major land cover classes (impervious surfaces, vegetation, bare soil, and water/shade) with both high spatial resolution and medium resolution images. The study showed that peak discharges derived from impervious surface information obtained from remote sensing data produced different results than traditional approaches, and sub-pixel estimation of impervious surface distribution can be used to substitute for the expensive high-resolution based approach for rainfall-runoff modeling. Mohapatra and Wu (2007) also used a three-layer feed forward back propagation neural network to estimate the percentage of impervious surfaces by creating activation level maps from high spatial resolution images (e.g. IKONOS), and the results indicated that the ANN model performed well in urban areas and is promising for impervious surface estimation from high spatial resolution images.

Although MLP has been widely used, some drawbacks have been raised by the previous research. For instance, how to design the number of hidden layers and the number of hidden layer nodes in the model are challenging issues. Although several methods have been suggested to estimate the appropriate number of hidden layer nodes, none of them have been universally accepted (Kavzoglu & Mather, 2003).

Another problem of MLP is that MLP requires the training sites to include both presence and absence data. The desired output must contain both true and false information, so that the network can learn all kinds of patterns in the study area to classify an image accordingly (Li & Eastman, 2006a). However, in some cases, absence data is not available. Therefore, MLP might not be suitable for those cases, and other ANN models should be used. Finally, MLP has the local minima problem in the training process, which significantly affects the accuracy of the result.

Self-organizing map (SOM) has not been applied as widely as MLP (Pal et al., 2005). However, SOM can be used for both supervised and unsupervised classification and has the properties for both vector quantization and vector projection (Li & Eastman, 2006a). SOM has been used for per-pixel classification and sub-pixel classification in

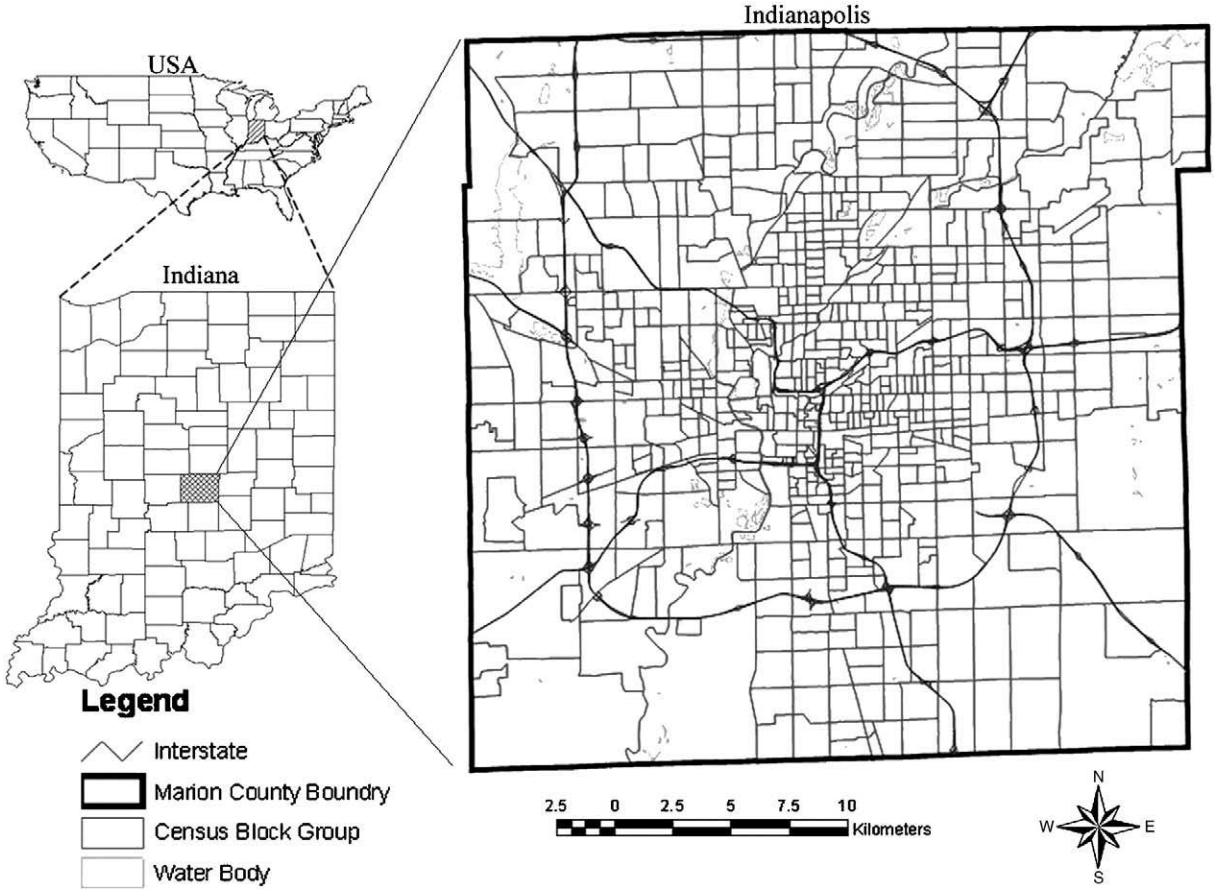

Fig. 1. Study area — Indianapolis city property (Marion County), Indiana, USA.

previous studies (Ji, 2000; Lee & Lathrop, 2006). Ji (2000) compared a Kohonen self-organizing feature map (KSOFM) and an MLP for LULC classification from remote sensing images at per-pixel level. Seven classes were selected, and the result showed that SOM provides a promising alternative to MLP neural network in per-pixel classification. Lee and Lathrop (2006) conducted a SOM to extract urban land cover from the Landsat ETM+ images at sub-pixel level. The result showed that SOM can generate promising 'soft' classification and has advantages over MLP.

The performances of SOM and MLP have not been compared in estimation and mapping of urban impervious surfaces. In mid-latitude areas, plant phenology has a significant influence on remote sensing of the environment. When the neural networks approaches are applied, how satellite images acquired in different seasons impact impervious surface estimation of various urban surfaces (such as commercial, residential, and suburban/rural areas) remains to be answered. In this paper, a sub-pixel classification method based on the Kohonen self-organizing feature map was adopted and applied to three Terra's ASTER images of Indianapolis, Indiana, United States, acquired in different seasons for impervious surface estimation. The MLP neural network was also applied to the same images in order to compare the results. Their performances were evaluated by conducting an accuracy assessment for the whole study area as well as for samples of commercial, residential, and suburban/rural areas. The rest of this paper is organized as follows: Section 2 describes the study area and the datasets used; methodology is discussed in Section 3; In Section 4, the results are presented; Section 5 discusses the problems that were encountered in this research as well as probable solutions; and Section 6 presents the conclusions.

2. Study area and datasets

Indianapolis/Marion County, Indiana, USA, was chosen as the study area (Fig. 1). The city is appropriate for this study because of

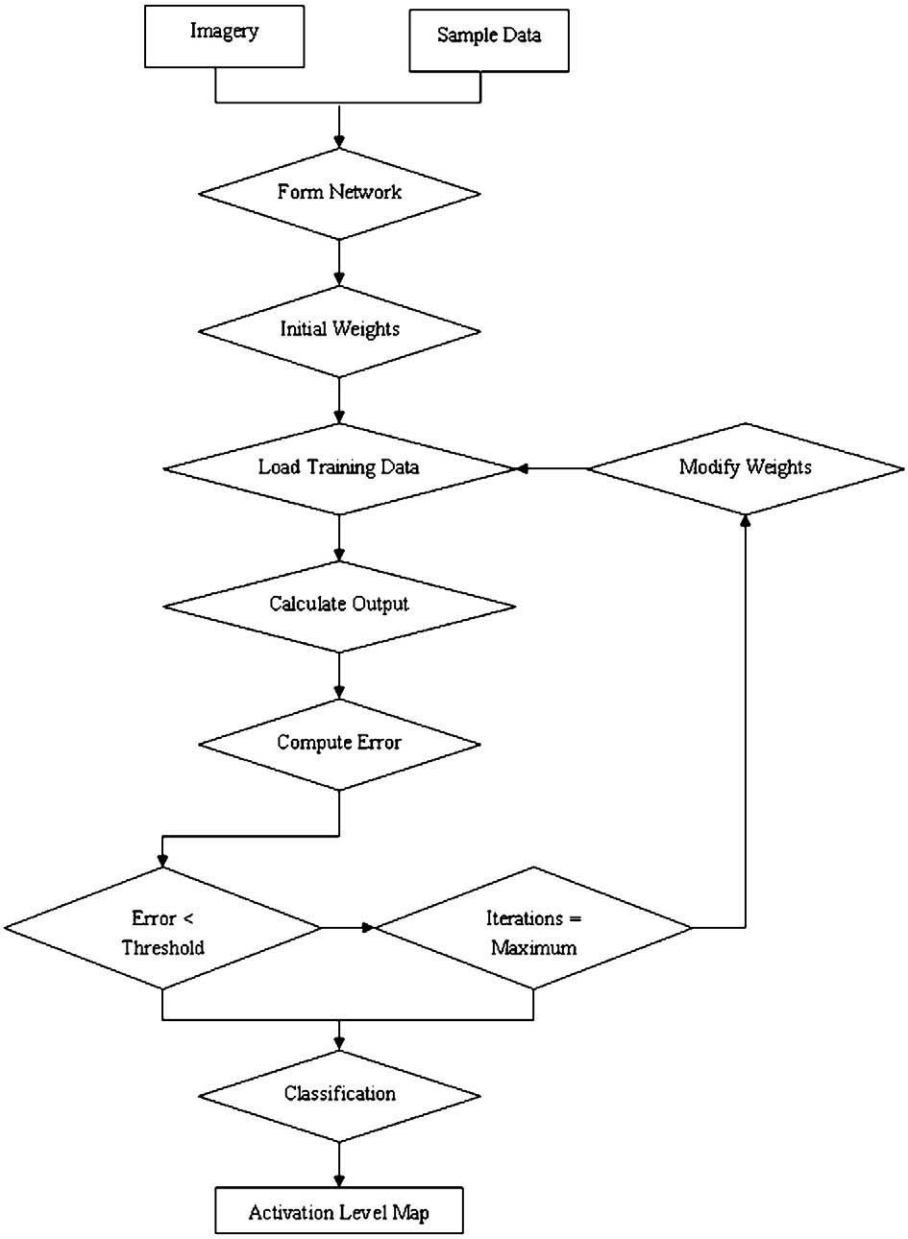

Fig. 2. The flowchart of MLP. (Images and training samples are first input into the model. Then, the MLP results are generated, and compared to the testing samples. If the difference is larger than the initialized threshold value, the weights are modified to minimize the difference between the actual and desired outputs. The process will be repeated until a predefined accuracy level or maximum iterations are reached.)

Table 1
The configuration of MLP.

Parameter	Value
Hidden layer nodes	4
Learning rate	0.16
Momentum factor	0.57
Sigmoidal constant *a*	14.48
Accurate rate (%)	95

three reasons. First, it is a single city without any significant impact from other large urban areas. Second, the city is located in a flat plain, relatively symmetrical, and expands in all direction. Finally, like many other American cities, Indianapolis is undergoing a rapid urban expansion with the increase in both population and area. The urban expansion can be characterized as the conversion of adjacent rural areas into impervious surfaces. Rapid changes of the landscape without prudent planning might lead to environmental degradation. Therefore, detailed impervious surface information is crucial to urban planning and environmental management in the city of Indianapolis.

Three ASTER images of Marion County, Indiana, which were acquired on April 5, 2004, June 16, 2001, and October 3, 2000, respectively, were used in this research. ASTER images have 14 bands with different spatial resolutions. Two visible bands and one NIR band have a spatial resolution of 15 m, 6 SWIR bands have 30-m spatial resolution, and 5 TIR bands have a spatial resolution of 90 m. All 14 bands were stacked together, and an image-to-image registration was conducted. The images were georectified to Universal Transverse Mercator (UTM) projection with NAD27 Clarke 1866 Zone 16, by using 1:24,000 Digital Raster Graphic (DRG) maps as the reference data. Approximately 40–50 ground control points were chosen for each image. The images were re-sampled to the spatial resolution of 15 m with the nearest-neighbor re-sampling algorithm. The root mean square errors (RMSE) for the geocorrection were all less than 0.3 pixels.

An aerial photo of Marion County with a spatial resolution of 0.14 m was used for classification refinement. The aerial photo was provided by the Indianapolis Mapping and Geographic Infrastructure System, and was acquired in April 2003. The coordinate system is Indiana State Plane East, Zone 1301, with North American Datum of 1983. The aerial photo was re-projected into the same coordinate system as the ASTER images.

3. Methodology

3.1. Multi-layer perceptron (MLP)

Artificial neural network (ANN) is an interconnected group of nodes using mathematical methods to process information. It is a self-adaptive system, which can change its structure based on the internal or external information. Many ANN models have been developed. The most popular one is the multi-layer perceptron (MLP) feed forward network (Kavzoglu & Mather, 2003). MLP, as the name indicates, has multiple layers. The three-layer structure was widely used, due to its capability to solve most image classification problems. The three layers include one input layer, one hidden layer, and one output layer. Each layer is composed of several nodes (artificial neurons). All the nodes are connected with each other, except for the nodes in the same layer. The input layer, the hidden layer and the output layer are used for data input, data processing, and data output, respectively. Specifically to image classification, the input layer represents the original image, and each input layer node represents one image band. The hidden layer is used for image classification and passing the results to the output layer. The output layer outputs classified images, and each output layer node represents one land cover/land use (LULC) class. ANN mimics the functions of human brains. Its learning ability comes from the learning algorithm, and the widely used one is back-propagation (BP), also known as delta rules. The process of learning can be described as that initial weights are initialized and assigned to each node. Training samples are then input into the model. Then, the ANN results are generated, and compared to the testing samples. If the difference is larger than the initialized threshold value, the weights are modified to minimize the difference between the actual and desired outputs. The process will be repeated until a predefined accuracy level or the maximum iterations are reached. The flowchart of MLP was shown in Fig. 2.

Constructing an applicable ANN model is a challenge. Many crucial parameters have to be set up manually, for example, the number of hidden layers and hidden layer nodes, learning rates, momentum factor, and training sites. The parameters have to be set up properly to find the global minimum of error function instead of a local minimum. The number of hidden layer nodes has a significant impact on classification accuracy. Too many hidden layer nodes will cause over-fitting of the model, while too few cannot identify the internal structure of the data

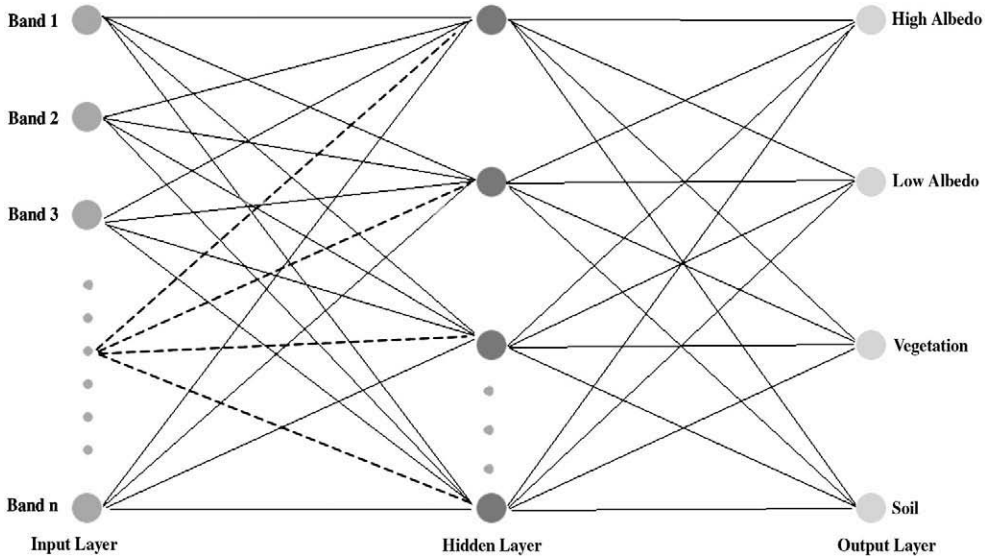

Fig. 3. The structure of the MLP neural network. (Three-layer structure, including: one input layer, one output layer, and one hidden layer. Input layer contains nine nodes corresponding to 9 ASTER bands, one hidden layer with four nodes for image classification, and one output layer with four nodes corresponding to four land cover classes: high albedo, low albedo, soil, and vegetation.)

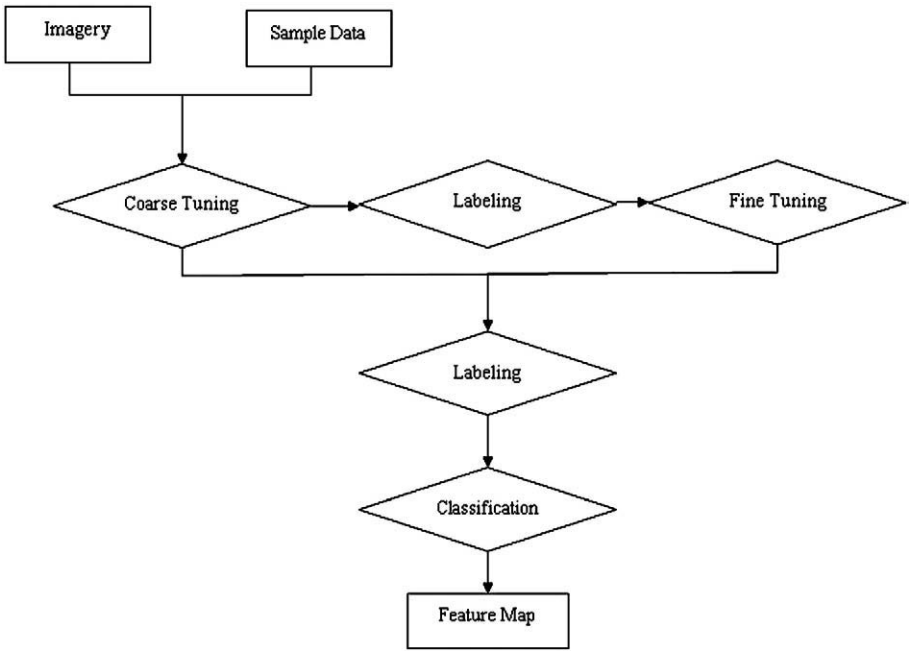

Fig. 4. The flowchart of SOM. (Images and training samples are first input into the model. A coarse tuning was conducted. The results can be used directly for classification to generate feature maps. The coarse tuning results also can be used for fine tuning. After fine tuning, the results were classified to generate feature maps.)

(Kavzoglu & Mather, 2003). If the learning rate is too high, the model will not be stable and cannot converge, but if it is too low, the model may end up finding a local minimum (Kavzoglu & Mather, 2003).

In this research, an MLP neural network with a BP learning algorithm was applied using IDRISI Andes program. The MLP classifier used the following algorithm to calculate the input that a single node j received:

$$net_j = \sum_i w_{ij} I_i \tag{1}$$

Where net_j refers to the input that a single node j receives; w_{ij} represents the weights between node i and node j; and I_i is the output from node i of a sender layer (input or hidden layer). Output from a node j was calculated as follows:

$$O_j = f\left(net_j\right) \tag{2}$$

The function f is usually a non-linear sigmoidal function.

In this research, an input layer with nine nodes corresponding to nine ASTER image bands (VNIR and SWIR), and one output layer with four nodes corresponding to four land cover classes, i.e., high albedo (e.g. concrete and sand), low albedo (e.g. water and asphalt), vegetation (e.g. grass and trees), and soil, were used. Albedo is defined as the ratio of diffusely reflected energy to the incident electromagnetic radiation. In general, high albedo materials are bright, and low albedo materials are dark in the image. The number of the hidden layer nodes could be calculated by the formula as follows:

$$N_h = INT\sqrt{N_i \times N_o} \tag{3}$$

Where N_h is the number of hidden layer nodes, h refers to the hidden layer, N_i is the number of input layer nodes, i refers to the input layer, N_o is the number of output layer nodes, and o refers to the output layer. The formula suggested that the number of hidden layer nodes should be six. However, after numerous tests, the network with four hidden layer nodes came out with the best result. Therefore, four hidden layer nodes were used in the model.

Thirty training samples for each land cover class, including high albedo, low albedo, soil, and vegetation, were manually selected from original images. Each sample had different size and contained a certain amount of pixels (e.g. >30 pixels) to make sure that there were enough pixels to be used for training and testing. All of the samples were distributed evenly in the image to represent the variety of spectral reflectance within the class. One hundred pixels per class were used for training, while another one hundred per class will be used for testing. The accuracy rate was set to 95% in this study. If 95% accuracy rate cannot be reached, a predefined iteration limit (10,000 times in this case) would stop the training process. Kavzoglu and Mather (2003) suggested that the value of a learning rate should be

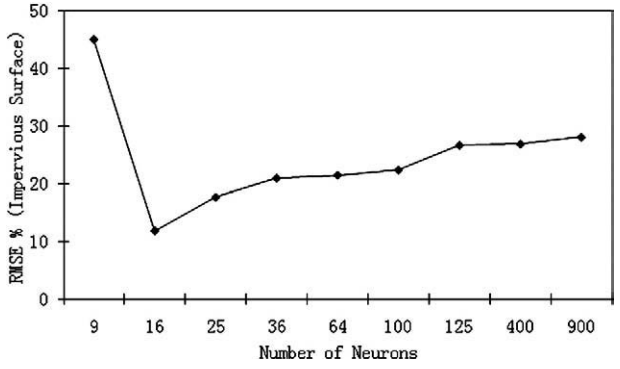

Fig. 5. Relationship between the map size and the impervious surface estimation (the June image was used as an example. The plot showed that when the maps size changed, the accuracy of impervious surface estimation varied. The map size of 4×4 was the best in this case).

Table 2
The configuration of SOM.

Parameter	Value
Input layer neuron number	9
Output layer neuron number	4×4
Initial neighborhood radius	6.66
Minimum learning rate	0.5
Maximum learning rate	1
Coarse tuning iterations	25,935

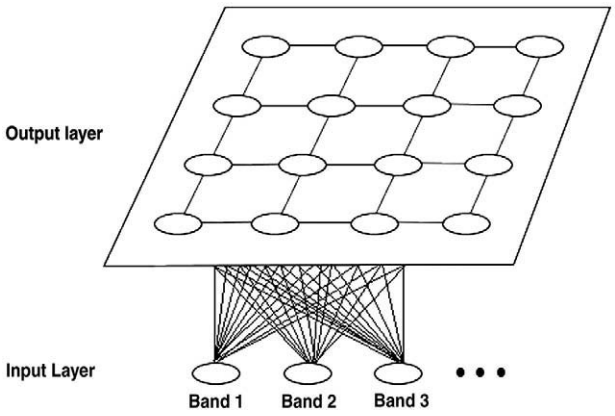

Fig. 6. The structure of the SOM neural network (Two layer structure, including: one input layer and one output layer. Input layer contains nine nodes corresponding to 9 ASTER bands, and the structure of the output layer is 4×4).

chosen between 0.1 and 0.2, while a momentum factor can be selected from a range between 0.5 and 0.6. The parameters used in this experiment were shown in Table 1.

The outputs of MLP are called activation level maps, and the number of activation level maps is equal to the number of output nodes. The value of each pixel in the activation level map represented the degree to which a pixel belongs to a class. The sum of activation values of all the land cover classes for any given pixel will not necessarily be one due to the outputs being obtained by a fuzzy process. In this research, four activation level maps were obtained, including high albedo, low albedo, vegetation, and soil. The fractions of impervious surface were obtained by adding high and low albedo activation level maps by using the method developed by Wu and Murray (2003). The structure of MLP used in this experiment was shown in Fig. 3.

3.2. Self-organizing map (SOM)

In this research, a sub-pixel classification based on Kohonen's self-organizing map (SOM) neural network was performed on the three ASTER images for impervious surface estimation. An SOM is composed of two layers: one input layer and one output layer. The input layer represents the input feature vector and contains neurons for each measurement dimension (e.g. image bands) and the output layer of SOM, also called the competitive layer, is usually organized as a two-dimensional array (typically square) of neurons. Each output layer neuron is connected to all the neurons in the input layer by synaptic weights, and the weights will be initialized randomly from 0 to 1.

The procedure of SOM begins with a coarse tuning in which the learning procedure will adjust the weights based on normalized input feature vectors and the lateral interaction between neurons in the output layer. During the learning process, the radius of the zone of lateral interaction will decrease. Coarse tuning will make input patterns with similar attributes cluster in the neuron layer, and neuron weights, which represent the underlying clusters and sub-clusters in the input data, will

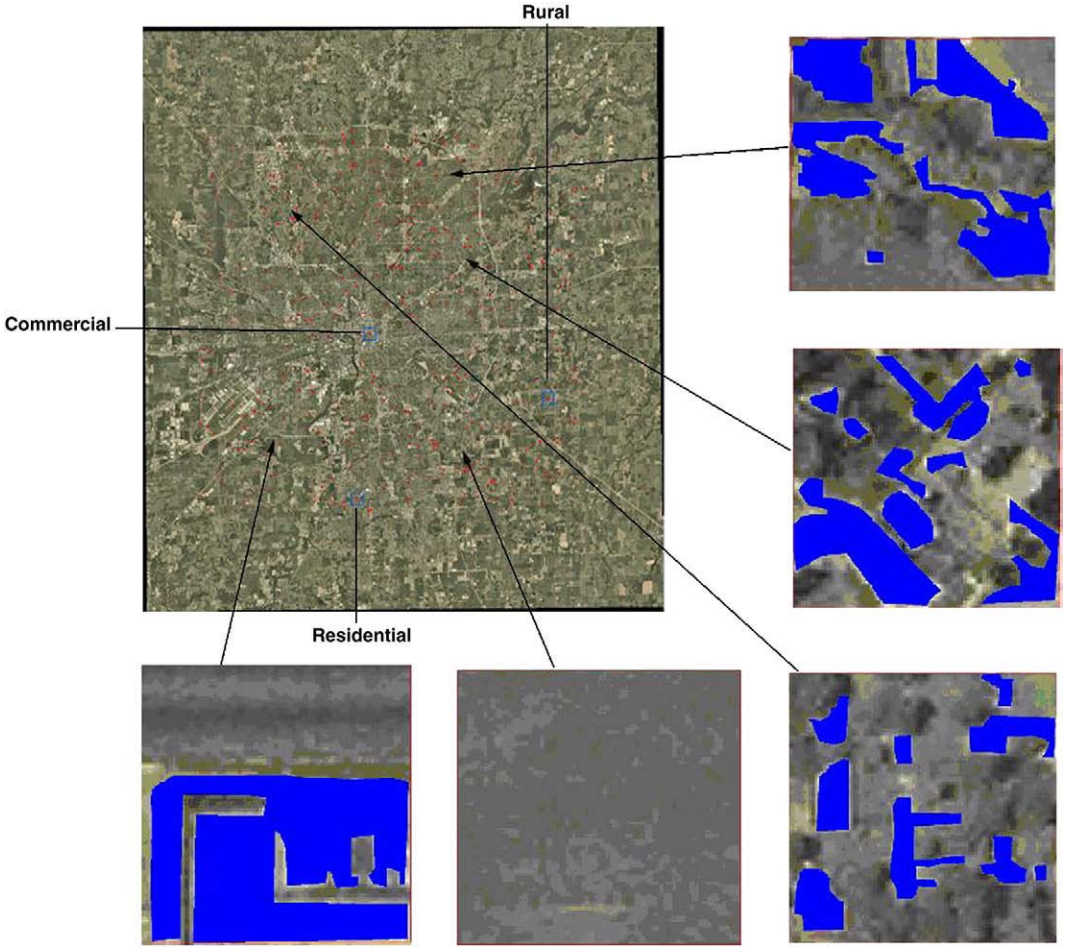

Fig. 7. Method of sample selection and obtaining reference data of impervious surfaces. (Red dots represent the samples, which are 6 pixels×6 pixels and 90 m×90 m. Five sample sites are enlarged and shown in this figure. The blue areas refer to the digitized impervious surfaces. Blue squares represent three test areas, including one commercial area, one residential area, and one rural area. Each has a dimension of 1 km×1 km.) (For interpretation of the references to color in this figure legend, the reader is referred to the web version of this article.)

be generated. After the SOM competitive layer was organized, a procedure called code book labeling phase will be performed to determine which class each output neuron belongs to. To achieve this, a procedure called majority voting was performed, in which training data will first be processed by coarse tuning, and the training site class which is most frequently assigned to a neuron, becomes its label. The next stage will be a fine tuning using learning vector quantizations (LVQs) to improve the discriminability of decision boundaries. Finally, each image pixel will be assigned the class of neuron that its reflectance patterns trigger (Li & Eastman, 2006b). The flowchart of SOM used in this experiment was shown in Fig. 4.

Numerous tests were conducted. The best result was generated by coarse tuning, instead of fine tuning. Therefore, in this experiment, only coarse tuning was conducted on the original images to yield the results. Different SOM map sizes were also tested in this study, and the results appeared to have significant differences (Fig. 5). The size of 4×4 appeared to be the best in the plot in terms of the accuracy of impervious surface estimation. Therefore, the map size of 4×4 was used for processing. Numerous parameters need to set up manually, such as initial neighborhood radius, minimum learning rate, and maximum learning rate. After numerous tests, the parameters which can yield the best result were selected, as shown in Table 2.

In this research, two algorithms based on SOM will be applied. One is called SOM commitment (SOM-C) and the other is SOM typicality (SOM-T). The first algorithm, SOM-C, is close to probability. During the labeling stage, a competitive layer neuron can be triggered by different patterns, and meanwhile, the same patterns may trigger different neurons as well. The degree of commitment indicating how much an input pattern belongs to a class can be measured by the following equation:

$$C_i = \frac{P_i(j)}{\sum_{i=1}^{m} P_i(j)} \tag{4}$$

Where $P_i(j)$ is the proportion of training site of class i, triggering neuron j, and $P_i(j)$ can be calculated as:

$$P_i(j) = \frac{f_i(j)}{N_i} \tag{5}$$

Where $f_i(j)$ is the frequency of neuron j triggered by pixels labeled as class i, and N_i is the total number of samples of class i in the training sites.

For the second algorithm, SOM-T, unlike SOM-C, the maximum triggering frequency within the underlying class of interest is used, instead of the sum of frequencies from classes or the accumulated frequency. The mathematical expression is shown as follows:

$$T_i = \frac{f_i(j)}{\max_i \{f_i(j)\}} \tag{6}$$

Unlike the SOM-C, the SOM-T algorithm considered the variability within the class (Li & Eastman, 2006a). In this paper, both algorithms were tested, and the best result was used to compare with the MLP neural network. Four feature maps were obtained, including high albedo, low albedo, vegetation, and soil. The fractions of impervious

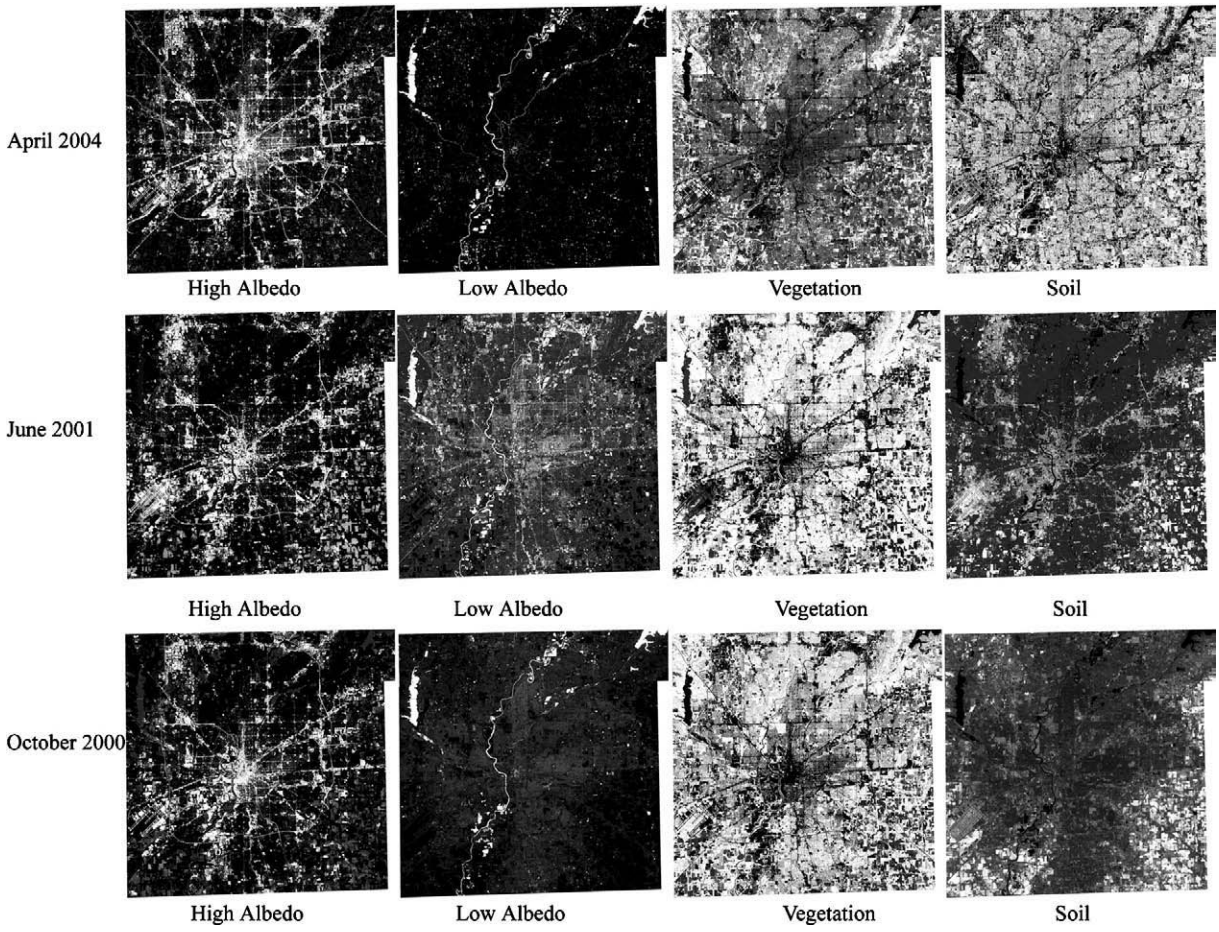

Fig. 8. Activation level maps (derived from ASTER images using the MLP neural network. Maps include high albedo, low albedo, vegetation and soil. The dates of images are April 5, 2004, June 16, 2001, and October 3, 2000, respectively).

surface were obtained by adding high and low albedo feature maps using the method presented by Wu and Murray (2003). The structure of SOM used in this study was shown in Fig. 6.

3.3. Accuracy assessment

A total of 400 sites of 90 m × 90 m were randomly sampled. We used high quality 2003 color orthophotos at 1:9600 scale, after being registered to the ASTER images, as the reference. The proportion of impervious surface coverage was calculated for each site. Fig. 7 illustrates the design of sample plots and the method for obtaining reference data by digitizing impervious surface polygons within selected samples. The RMSE, the mean average error (MAE), and the coefficient of determination (R^2) were then calculated to indicate the accuracy of impervious surface estimation. Below were the equations used:

$$\mathrm{RMSE} = \sqrt{\frac{\sum_{i=1}^{N}\left(\hat{I}_i - I_i\right)^2}{N}} \tag{7}$$

$$\mathrm{MAE} = \frac{1}{N}\sum_{i=1}^{N}\left|I_i - \hat{I}_i\right| \tag{8}$$

$$R^2 = \frac{\sum_{i=1}^{N}\left(\hat{I}_i - \bar{I}\right)}{\sum_{i=1}^{N}\left(I_i - \bar{I}\right)^2} \tag{9}$$

where $\hat{I}_i$ is the estimated impervious surface fraction for sample i; I_i is the impervious surface proportion computed from the aerial photo; $\bar{I}$ is the mean value of the samples; and N is the number of samples.

Three test areas were selected for further evaluation of the performance of the SOM and the MLP in handling the mixed pixels. These areas included one commercial area, one residential area, and one rural area. The logic behind the selection of the three areas was that the residential area contained a large portion of mixed pixels, while the commercial area and the rural area contained less mixed pixels. The results provided a direct evidence for which algorithm, the SOM or the MLP, was better in coping with mixed pixels. For the test areas, each was 1 km × 1 km. In each area, twenty samples, which were 90 m × 90 m, were randomly selected for the accuracy assessment.

4. Results

In this paper, both the SOM and the MLP neural network were conducted on the three ASTER images for impervious surface estimation. Four activation level maps and four feature maps of high albedo, low albedo, vegetation, and soil were generated for each image (Figs. 8 and 9). The activation level maps and the feature maps appropriately delineate the spatial pattern of each land cover type in the study area. Impervious surface maps were yielded by the method that was discussed above. The same process of removing spectrally confused materials (e.g. water, shade, and dry soils) was performed on all the impervious surface maps.

Fig. 10 illuminates the impervious surfaces extracted from the three ASTER images by the two algorithms. Although there were slight differences between the impervious surface maps, they shared similar spatial patterns of impervious surface distribution. Most of the impervious surfaces were located in the central business district (CBD) area and distributed along the transportation lines. An accuracy

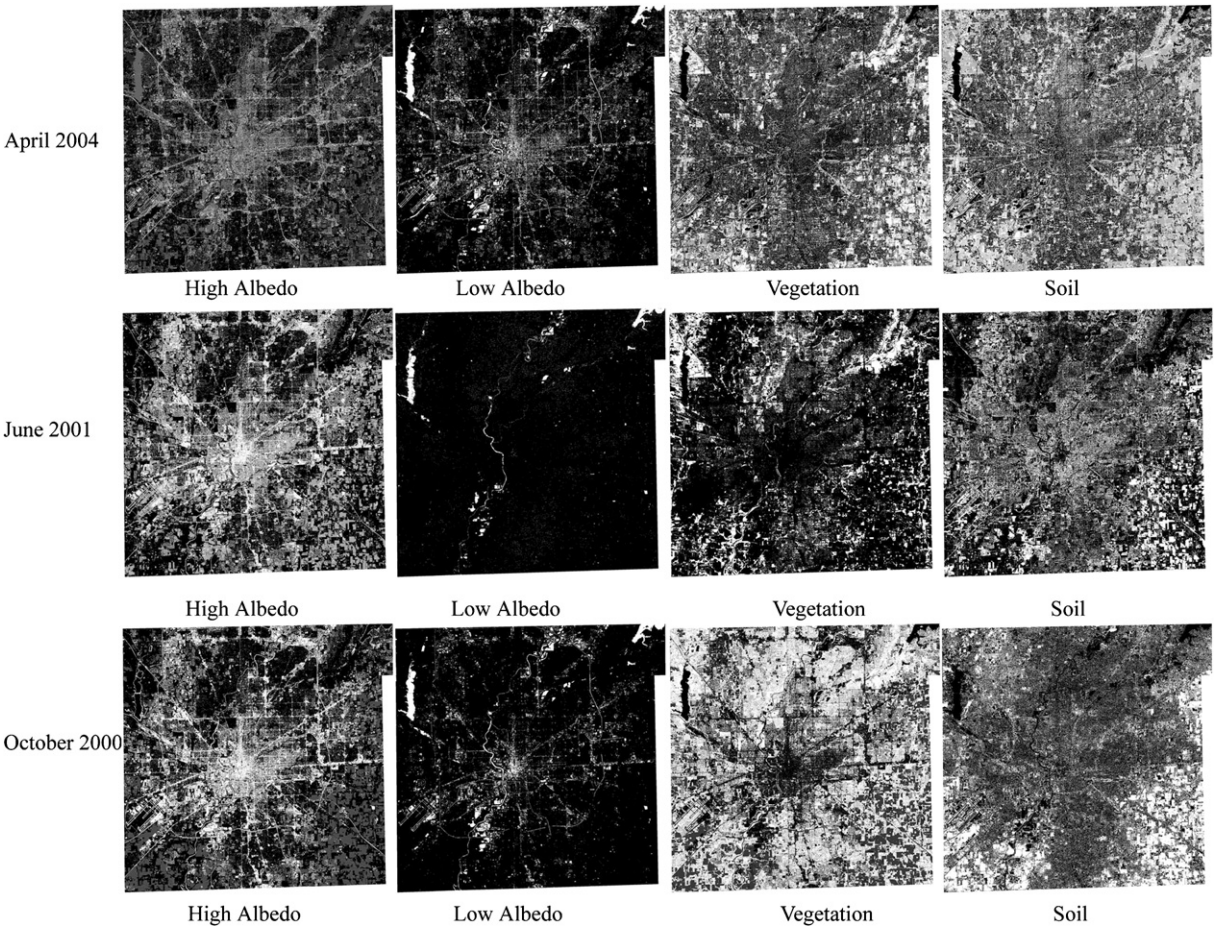

Fig. 9. Feature maps. (Four feature maps were obtained, including high albedo, low albedo, vegetation, and soil.)

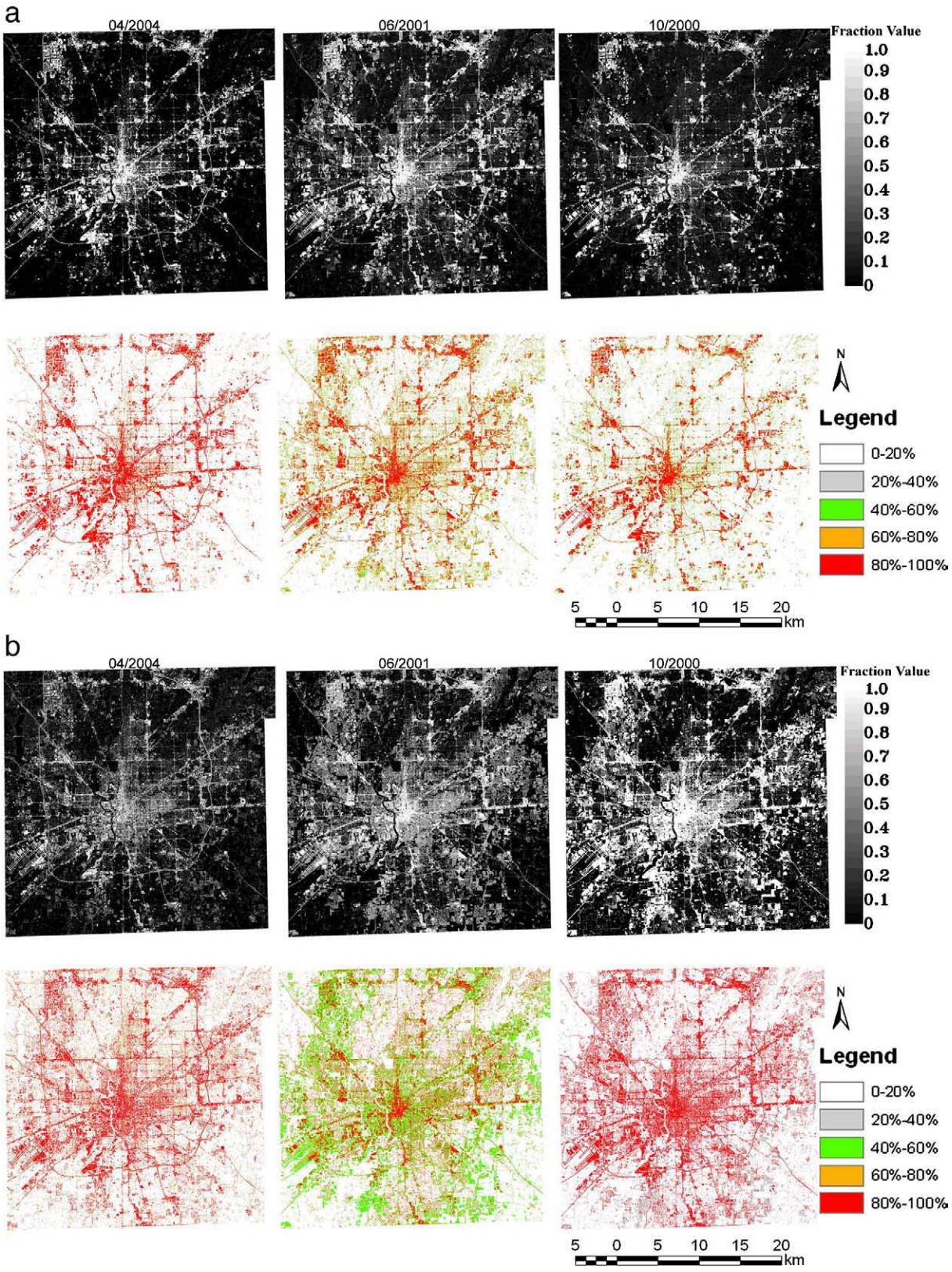

Fig. 10. Final impervious surface maps of Indianapolis, U.S.A. Color maps were produced by classify the data into five categories with equal intervals. (a) Impervious surface maps generated using MLP; and (b) Impervious surface maps generated using the SOM.

assessment was conducted to evaluate the results. Table 3 showed that the SOM generated slightly better results than MLP for all images. For the June image, MLP yielded a result with an RMSE of 12.3%, an MAE of 9.0%, and an R^2 of 0.771. The SOM generated the result with an RMSE of 11.8%, an MAE of 8.0%, and an R^2 of 0.775. For the April image, MLP yielded a result with an RMSE of 19.6%, an MAE of 13.4%, and an R^2 of 0.586. The SOM generated the result with an RMSE of 19.4%, an MAE of 14.1%, and an R^2 of 0.527. For the October image, MLP yielded a

Table 3
Accuracy assessment of impervious surface maps.

Algorithm	Date of image	RMSE (%)	MAE (%)	R^2
MLP	April 2004	19.6	13.4	0.586
	June 2001	12.3	9.0	0.771
	Oct. 2000	18.7	12.7	0.581
SOM	April 2004	19.4	14.1	0.527
	June 2001	11.8	8.0	0.775
	Oct. 2000	17.2	11.4	0.616

result with an RMSE of 18.7%, an MAE of 12.7%, and an R^2 of 0.581. The SOM generated the result with an RMSE of 17.2%, an MAE of 11.4%, and an R^2 of 0.616.

An accuracy assessment was also conducted for three selected areas, including one commercial area, one residential area, and one rural area (Table 4). In the residential area, more accurate result was yielded by the SOM, which indicates that the SOM was more effective in coping with the mixed pixels than the MLP, because the residential area prevailed with mixed pixels. Results obtained from the commercial area possessed very high RMSE values due to the prevalence of shade, which indicates that both algorithms cannot handle the shade problem well. The lowest RMSE value was obtained from the rural area due to containing of less mixed pixels and shade. In the rural area, the two methods generated quite different results. The SOM tended to confuse the dry soils with impervious surfaces, and MLP can differentiate the impervious surfaces from dry soil better than SOM. The feature maps and the activation level maps showed that more dry soils were included in the high albedo image of the feature maps than that of the activation level maps. Fig. 11 shows impervious surface maps derived in the three selected areas.

The results further show that there were seasonal differences in which the June image appeared to be the best for impervious surface extraction due to plant phenology. The quality of the impervious surface map was slightly improved by the SOM over the MLP for the June image. However, there were significant improvements by the SOM for the April and October images in terms of statistical accuracy. Mapping impervious surfaces were the reverse of mapping vegetation abundance. The more the vegetation, the less the confusion in estimating impervious surfaces. This is because vegetation had a very different spectral signature from impervious surfaces. When tree leaves fell off, remote sensors tended to sense the energy from tree trunks and twigs. And when crops were harvested, the bare soil was exposed. The spectral signature of dry soils was similar to that of bright impervious surfaces. This confusion could lead to a less accurate estimation of impervious surfaces. This is why the June image achieved a better result than the April and October ones. In Indiana on June 16, grass had already grown, tree canopies had been fully developed, and crops had started to grow. The vegetation was abundant at that time. Nevertheless, on April 5, the tree canopy had not appeared yet. Grass and pasture were in their very early stages, while there was no crop. Soils in the fields were sometimes mixed with crop stems, and at other times, they were exposed. On October 3, grass and tree canopies began to degrade a little, but most of them were still there with good conditions. Most crops had been harvested or turned yellow, and croplands were clearly identifiable due to the change in their spectral signatures. The vegetation abundance in October was between April and June. The change of vegetation abundance and associated changes in its spectral signature within a year had an obvious impact on image analysis in general, and in impervious surface estimation and mapping in particular.

Scatter plots of the accuracy assessment (Fig. 12) showed that there was overestimation in the less developed area, while underestimation in areas with high proportions of impervious surface coverage, and this phenomenon existed in most of the impervious surface maps, regardless of the SOM or the MLP methods being used. This can be explained by the loss of impervious surfaces covered by shadows in the central business district (CBD) area and the confusion of dry soils in the rural areas during the extraction.

5. Discussions

The MLP neural network is widely used in the remote sensing studies (Atkinson & Tatnall, 1997). It also has been applied for impervious surface estimation with a fair amount of success (Chormanski et al., 2008; Mohapatra & Wu, 2007). However, the MLP neural network contains some limitations. First, MLP is sensitive to the network structure, i.e., the hidden layer number and its node number. The number of hidden layer nodes defines the complexity of the neural network, significantly affecting the classification accuracy and the training time. Although there are several methods which have been suggested to estimate the appropriate number of hidden layer nodes, none of them have been universally accepted (Kavzoglu & Mather, 2003). Second, MLP requires the training sites to include both presence and absence data. The desired output must contain both true and false information, so that the network can learn all kinds of patterns in the study area to classify accordingly (Li & Eastman, 2006a). Third, MLP has the local minima problem. The training process stops at a local minimum instead of the global minimum. Fourth, the learning process of the BP algorithm is time-consuming (Tzeng et al., 1994). Finally, the training process of the BP algorithm is not consistent.

Unlike MLP, SOM can overcome those drawbacks. First, SOM is a two-layer structure, including one input layer and one output layer. Therefore, the dilemma of determining the hidden layer size is avoided. Second, SOM is capable of coping with presence-only data (Li & Eastman, 2006a). Third, the SOM is not affected by the local minima problem in the training process and is insensitive to the structure of the codebook vector map (Lee & Lathrop, 2005). Fourth, the feature map is a faster learner. Finally, the feature map is also more consistent than the BP algorithm (Ji, 2000).

Although the SOM has advantages over the MLP neural network, the classification process of the SOM is slower than the MLP, and the accuracy level is heavily related to the size of the feature map. In this paper, two algorithms, SOM commitment and SOM typicality, were conducted. However, the impact between these two algorithms on the performance of the SOM neural networks was not as much as changing the SOM map size. Different SOM map sizes were tested in this study, and the results appeared to have significant differences. The sensitivity analysis results showed that too few or too many neurons significantly increased the RMSE of the estimation result. Therefore, an appropriate size of the SOM map needs to be established to achieve the best result of impervious surface estimation. The number of the samples selected for each class also affects the performance of the SOM neural network. Classes with more training samples will be more accurately distinguished, because more codebooks were occupied and few samples results in fewer codebooks being activated during training (Ji, 2000). Therefore, the number of samples selected for each class needs to be balanced.

The difficulties also came from the spectrally confused features (e.g. water, shade, and dry soils) in the satellite images. Water and

Table 4
Accuracy Assessment of selected test areas.

RMSE (%)		Commercial	Residential	Rural
MLP	April 2004	20.3	26.7	16.1
	June 2001	19.6	12.0	10.9
	Oct. 2000	23.9	24.4	15.0
SOM	April 2004	28.9	22.0	16.3
	June 2001	18.2	11.9	11.7
	Oct. 2000	26.0	17.5	15.3

shade often share similar spectral characteristics with dark impervious surfaces, while dry soils tend to be confused with bright impervious surfaces. The spectral similarity brings more difficulties to distinguish impervious surfaces from non-impervious materials. The spectral similarity would be more complicated when plant phenology is considered (Weng & Hu, 2008).

6. Conclusions

In this paper, an SOM and an MLP neural network were applied to three ASTER images covering Marion County, Indiana, U.S.A., acquired on April 5, 2004, June 16, 2001, and October, 3 2000, respectively, to evaluate and compare these two methods in terms of the effectiveness

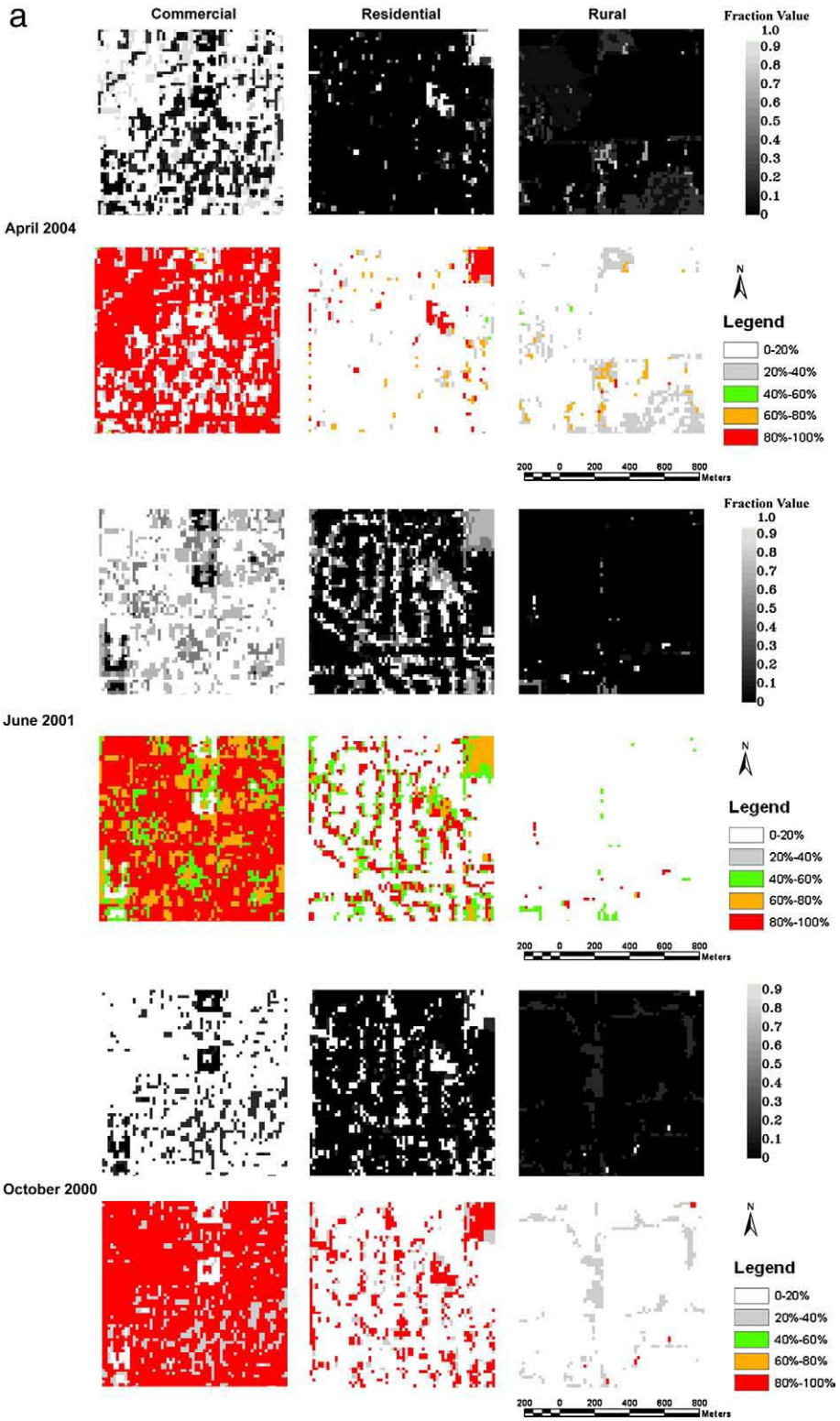

Fig. 11. Impervious surface maps in three selected areas, including one commercial area, one residential area, and one rural area. (a) Impervious surface maps generated using the SOM; and (b) Impervious surface maps generated using MLP.

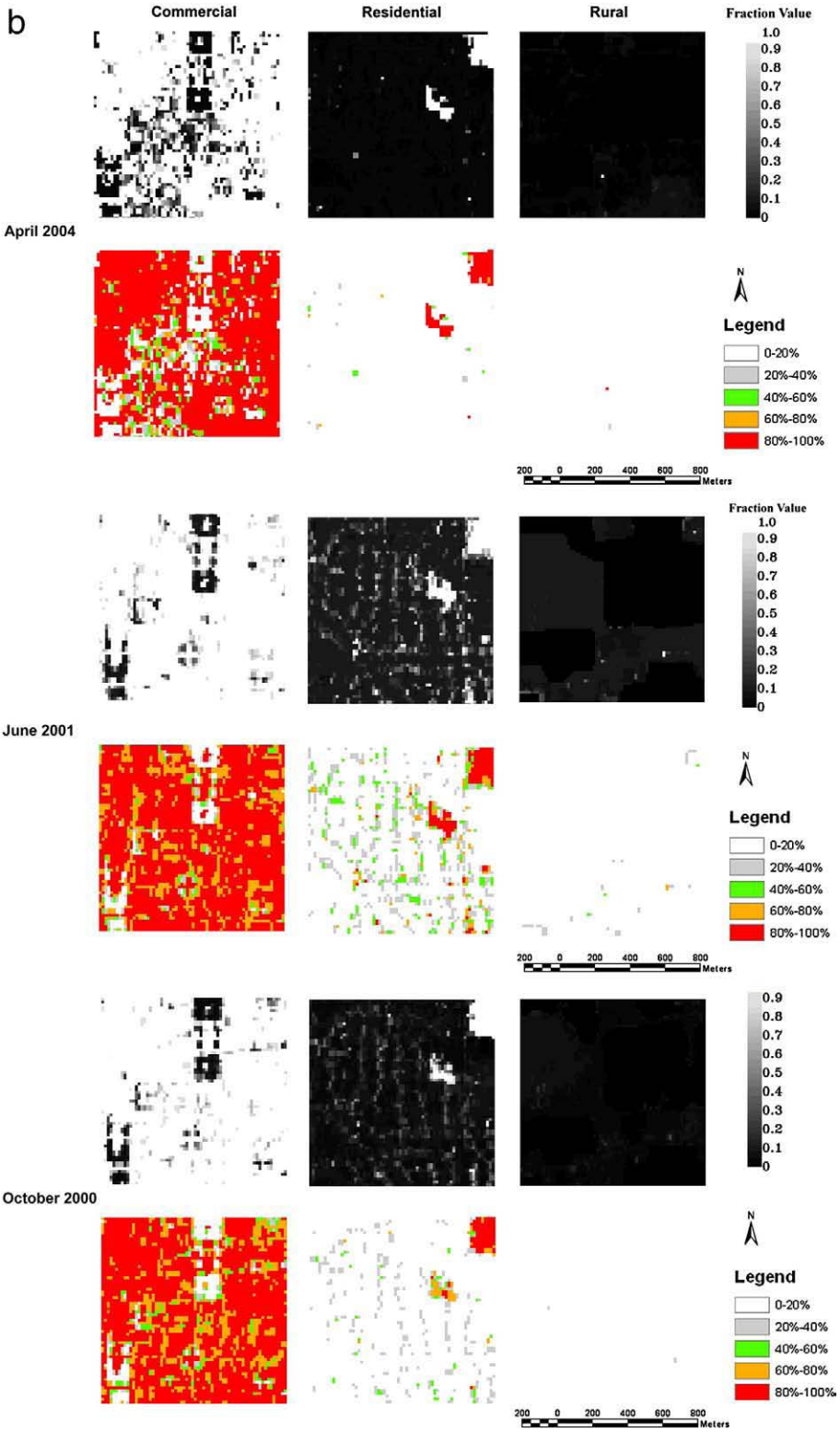

Fig. 11 (*continued*).

in estimation and mapping of urban impervious surfaces. Six impervious surface maps were yielded. The results indicated that all maps can generally delineate the spatial patterns of the impervious surface distribution within the study area. An accuracy assessment was carried out. The RMSE, the MAE, and the R^2 were calculated for each map. The results indicated that the SOM generated a slightly better result of impervious surface estimation than the MLP neural network.

The results of our study support previous observations by Ji (2000) and Lee and Lathrop (2006) that the SOM algorithm provides a promising alternative to the MLP neural network for image classification at both per-pixel and sub-pixel level. Although SOM generated

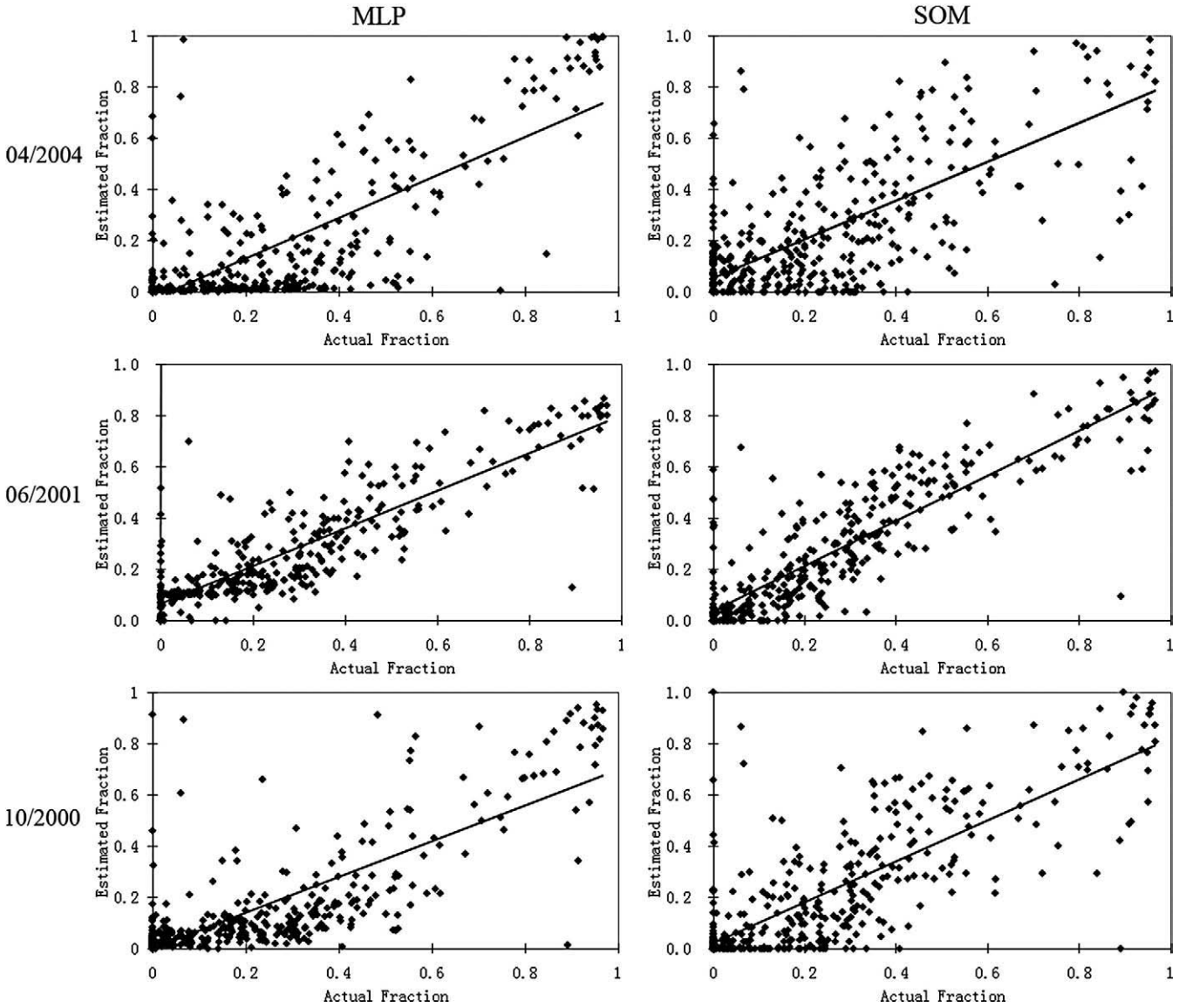

Fig. 12. Scatter plots of accuracy assessment results. (The scatter plots indicate that there was overestimation in the less developed area, while underestimation in area with high proportions of impervious surface coverage. This phenomenon existed in all the impervious surface maps, regardless of MLP or SOM method being used.)

better results than MLP in this case study, if the SOM can consistently yield better results than MLP is still unknown. More study areas need to be tested in the future study. Moreover, the impact of different map sizes on the impervious surface estimation is significant. Too many or too few neurons in the SOM model significantly increased the RMS error of the impervious surface estimation results. Therefore, an appropriate size of the SOM map needs to be established to achieve the best results of impervious surface estimation.

Acknowledgments

This research is supported by National Science Foundation (BCS-0521734) for a project entitled "Role of Urban Canopy Composition and Structure in Determining Heat Islands", and by Indiana State University Research Committee (UNR267) for a project entitled "A Protocol for Measuring and Validating Impervious Surface Data Derived from Medium Resolution Remote Sensing Imagery". We are grateful for three anonymous reviewers for their constructive comments and suggestions, and for Drs. Paul Mausel and James Speer for proof-reading this manuscript and useful comments on an earlier version of the manuscript.

References

Arnold, C. L., & Gibbons, C. J. (1996). Impervious surface coverage: The emergence of a key environmental indicator. *Journal of the American Planning Association*, *62*, 243—258.

Atkinson, P. M., & Tatnall, A. R. L. (1997). Introduction: Neural networks in remote sensing. *International Journal of Remote Sensing*, *18*, 699—709.

Bauer, M. E., Heinert, N. J., Doyle, J. K., & Yuan, F. (2004). Impervious surface mapping and change monitoring using Landsat remote sensing. *Proceedings of ASPRS annual conference, May 24–28, Denver, Colorado*.

Chattopadhyay, S., & Bandyopadhyay, G. (2007). Artificial neural network with backpropagation learning to predict mean monthly total ozone in Arosa, Switzerland. *International Journal of Remote Sensing*, *28*(20), 4471—4482.

Chormanski, J., Voorde, T. V. D., Roeck, T. D., Batelaan, O., & Canters, F. (2008). Improving distributed runoff prediction in urbanized catchments with remote sensing based estimates of impervious surface cover. *Sensors*, *8*, 910—932.

Civico, D. L., & Hurd, J. D. (1997). Impervious surface mapping for the state of Connecticut. *Proceedings of ASPRS/ACSM annual convention, April 7–10, Seattle, Washington, Vol. 3* (pp. 124—135).

Corsini, G., Diani, M., Grasso, R., De Martino, M., Mantero, P., & Serpico, S. B. (2003). Radial basis function and multilayer perceptron neural networks for sea water optically active parameter estimation in case II waters: A comparison. *International Journal of Remote Sensing*, *24*(20), 3917.

Flanagan, M., & Civco, D. L. (2001). Subpixel impervious surface mapping. *Proceedings of 2001 ASPRS annual convention, April 23–27, St. Louis, MO*.

Foody, G. M., Lucas, R. M., Curran, P. J., & Honzak, M. (1997). Non-linear mixture modelling without end-members using an artificial neural network. *International Journal of Remote Sensing*, *18*, 937—953.

Galli, J. (1991). Thermal impacts associated with urbanization and stormwater management best management practices. *Metropolitan Washington Council of Governments*. Washington D. C.: Maryland Department of Environment. 188 p.

Hasse, J. E., & Lathrop, R. G. (2003). Land resource impact indicators of urban sprawl. *Applied Geography*, *23*(2–3), 159—175.

Ingram, J. C., Dawson, T. P., & Whittaker, R. J. (2005). Mapping tropical forest structure in southeastern Madagascar using remote sensing and artificial neural networks. *Remote Sensing of Environment*, *94*(4), 491—507.

Jae-Dong, J., Viau, A. A., Francois, A., & Bartholome, E. (2006). Neural network application for cloud detection in SPOT VEGETATION images. *International Journal of Remote Sensing*, *27*(3/4), 719—736.

Ji, C. Y. (2000). Land-use classification of remotely sensed data using Kohonen self-organizing feature map neural networks. *Photogrammetric Engineering & Remote Sensing*, *66*, 1451—1460.

Kavzoglu, T., & Mather, P. M. (2003). The use of backpropagating artificial neural networks in land cover classification. *International Journal of Remote Sensing*, *24*(23), 4907—4938.

Lee, S., & Lathrop, R. G. (2005). Sub-pixel estimation of urban land cover components with linear mixture model analysis and Landsat Thematic Mapper imagery. *International Journal of Remote Sensing*, *26*(22), 4885—4905.

Lee, S., & Lathrop, R. G. (2006). Subpixel analysis of Landsat ETM+ using self-organizing map (SOM) neural networks for urban land cover characterization. *IEEE Transactions on Geoscience and Remote Sensing*, *44*(6), 1642—1654.

Li, X., & Yeh, A. G. -O. (2002). Neural-network-based cellular automata for simulating multiple land use changes using GIS. *International Journal of Geographical Information Science*, *16*(4), 323—343.

Li, Z., & Eastman, J. R. (2006). Commitment and typicality measurements for the self-organizing map. *Proceedings of SPIE — The International Society for Optical Engineering, Bellingham, WA* 64201I-1-64201I-4.

Li, Z., & Eastman, J. R. (2006). The nature and classification of unlabelled neurons in the use of Kohonen's self-organizing map for supervised classification. *Transactions in GIS*, *10*(4), 599.

Linderman, M., Liu, J., Qi, J., An, L., Ouyang, Z., Yang, J., & Tan, Y. (2004). Using artificial neural networks to map the spatial distribution of understorey bamboo from remote sensing data. *International Journal of Remote Sensing*, *25*(9), 1685—1700.

Lu, D., & Weng, Q. (2006). Spectral mixture analysis of ASTER images for examining the relationship between urban thermal features and biophysical descriptors in Indianapolis, Indiana, USA. *Remote Sensing of Environment*, *104*(2), 157—167.

Mohapatra, R. P., & Wu, C. (2007). Sub-pixel imperviousness estimation with IKONOS image: an artificial neural network approach. In Q. Weng & B. Rato (Eds.), *Remote Sensing of Impervious Surfaces*. FL: CRC Press, Taylor and Francis Group, (pp. 21–38).

Pal, N. R., Laha, A., & Das, J. (2005). Designing fuzzy rule based classifier using self-organizing feature map for analysis of multispectral satellite images. *International Journal of Remote Sensing*, *26*(10), 2219—2240.

Schiller, H., & Doerffer, R. (1999). Neural network for emulation of an inverse model operational derivation of Case II water properties from MERIS data. *International Journal of Remote Sensing*, *20*(9), 1735—1746.

Schueler, T. (1994). The importance of imperviousness. *Watershed Protection Techniques*, *1*(3), 100—111.

Slonecker, E. T., Jennings, D. B., & Garofalo, D. (2001). Remote sensing of impervious surfaces: A review. *Remote Sensing Reviews*, *20*(3), 227—255.

Small, C. (2001). Estimation of urban vegetation abundance by spectral mixture analysis. *International Journal of Remote Sensing*, *22*(7), 1305—1334.

Small, C. (2003). High spatial resolution spectral mixture analysis of urban reflectance. *Remote Sensing of Environment*, *88*(1–2), 170—186.

Tzeng, Y. C., Chen, K. S., Kao, W. L., & Fung, A. K. (1994). A dynamic learning neural network for remote sensing applications. *IEEE Transactions on Geoscience and Remote Sensing*, *32*(5), 1096—1102.

Weng, Q., & Hu, X. (2008). Medium spatial resolution satellite imagery for estimating and mapping urban impervious surfaces using LSMA and ANN. *IEEE Transactions on Geoscience and Remote Sensing*, *46*(8), 2397—2406.

Wu, C. (2004). Normalized spectral mixture analysis for monitoring urban composition using ETM+ imagery. *Remote Sensing of Environment*, *93*, 480—492.

Wu, C., & Murray, A. T. (2003). Estimating impervious surface distribution by spectral mixture analysis. *Remote Sensing of Environment*, *84*, 493—505.

Yang, L., George, X., Klaver, J. M., & Deal, B. (2003). Urban land-cover change detection through sub-pixel imperviousness mapping using remotely sensed data. *Photogrammetric Engineering and Remote Sensing*, *69*(9), 1003—1010.

Yang, L., Huang, C., Homer, C. G., Wylie, Bruce K., & Coan, M. J. (2003). An approach for mapping large-area impervious surfaces: Synergistic use of Landsat-7 ETM+ and high spatial resolution imagery. *Canadian Journal of Remote Sensing*, *29*(2), 230—240.

Yuan, F., & Bauer, M. E. (2007). Comparison of impervious surface area and normalized difference vegetation index as indicators of surface urban heat island effects in Landsat imagery. *Remote Sensing of Environment*, *106*(3), 375—386.

Zhang, J., & Foody, G. M. (2001). Fully-fuzzy supervised classification of sub-urban land cover from remotely sensed imagery: Statistical and artificial neural network approaches. *International Journal of Remote Sensing*, *22*(4), 615—628.

Zhang, Y., Pulliainen, J., Koponen, S., & Hallikainen, M. (2002). Application of an empirical neural network to surface water quality estimation in the Gulf of Finland using combined optical data and microwave data. *Remote Sensing of Environment*, *81*(2–3), 327—336.